Bidirectional Backscatter NOMA Schemefor Efficient CDRT Systems

Rongfei Hu[1,2], Yao Xu[1(✉)], Jianyue Zhu[1], Jichong Guo[3], Shaobo Jia[4], Yi Lou[5], and Chengzhao Shan[5]

[1] Nanjing University of Information Science and Technology, Nanjing 210044, China
yaoxu@nuist.edu.cn
[2] NUIST-TianChang Research Institute, Tianchang 239300, China
[3] Suzhou University of Science and Technology, Suzhou 215009, China
[4] Zhengzhou University, Zhengzhou 450001, China
[5] Harbin Institute of Technology, Harbin 150001, China

Abstract. Non-orthogonal multiple access (NOMA) based coordinated direct and relay transmission (CDRT) is recognized as one of the enabling technologies for effectively enhancing spectral efficiency and coverage range in mobile communication systems. However, most conventional NOMA based CDRT schemes only support cellular data transmission. To simultaneously support both cellular and Internet of Things (IoT) data transmission and further improve the spectral efficiency of the system, this paper proposes a novel bidirectional backscatter NOMA scheme for CDRT systems. Specifically, the proposed scheme utilizes both uplink NOMA and downlink NOMA to facilitate the sharing of spectrum and time resources between cellular information and IoT data reflected by users. To accurately characterize the effectiveness of the proposed scheme, the closed-form expressions for the ergodic sum capacity (ESC) are derived. Simulation experiments validate the correctness of theoretical analysis and demonstrate that the proposed scheme can achieve better ESC performance than the conventional NOMA based CDRT and orthogonal multiple access.

Keywords: Non-orthogonal multiple access · Coordinated direct and relay transmission · Backscatter communication · Ergodic sum capacity

This work was supported in part by the Natural Science Foundation of Jiangsu Province under Grants BK20220438 and BK20220439; in part by National Natural Science Foundation of China under Grant 62301268; in part by the Natural Science Foundation of the Higher Education Institutions of Jiangsu Province under Grants 22KJB510033 and 22KJB10005; and in part by the Startup Foundation for Introducing Talent of NUIST under Grant 2023r015.

H.-H. Chen and W. Meng (Eds.): WiSATS 2024, LNICST 605, pp. 214–225, 2025.
https://doi.org/10.1007/978-3-031-86196-3_18

1 Introduction

The sixth generation (6G) mobile communication urgently requires enhancements in system spectral efficiency and communication coverage to support diverse vertical applications [1–3]. Integrating non-orthogonal multiple access (NOMA) and coordinated direct and relay transmission (CDRT) enables the exploitation of power domain NOMA to serve multiple users within the same time/frequency/code resources, while also supporting direct transmission and relay communication simultaneously [4,5]. Thus, NOMA based CDRT, renowned for its high spectral efficiency and broad coverage, has become a focal point of academic interest in recent years. For instance, significant research efforts have been dedicated to studying various aspects of NOMA based CDRT systems, such as efficient aggregate transmission [6], physical layer security [7], and high speed mobile applications [8]. However, existing NOMA based CDRT schemes encounter challenges due to limited spectrum resources and inter-user interference. These challenges hinder the simultaneous support for the fusion transmission of cellular information and low rate Internet of Things (IoT) sensing information, thus impeding the heterogeneous fusion development of future mobile communications.

Fortunately, backscatter NOMA offers a novel approach to address the aforementioned issues. Backscatter communication utilizes ambient radio frequency (RF) signals and adjusts the matching state between load impedance and antenna impedance to reflect low rate IoT information to the receiver without consuming additional energy [9]. When the receiver is equipped with both the conventional transceiver circuits and backscatter circuits, it can decode its own information using a portion of the received signal, while the remaining part is used to modulate its own information for transmission [10].

Motivated by these observations, this paper proposes a novel bidirectional backscatter NOMA scheme for CDRT systems to simultaneously support the fusion transmission of cellular and IoT information, thereby further enhancing spectral efficiency. The contributions of this paper are summarized as follows. (1) This paper proposes a bidirectional backscatter NOMA scheme for CDRT systems. In the proposed scheme, the base station (BS) collects IoT information from both the cell center user (CCU) and relay user (RU) using uplink backscatter NOMA, and then the CCU collects IoT information from the RU and cell edge user (CEU). Meanwhile, the BS employs downlink NOMA to serve the three users in the two time slots. (2) To characterize the performance of the proposed scheme, we derived the closed-form expressions for the ergodic sum capacity (ESC) using Gamma-Gamma distribution and Gaussian-Chebyshev quadrature. (3) Simulations demonstrate that the proposed scheme achieves superior ESC performance compared with the conventional NOMA based CDRT and orthogonal multiple access (OMA) under various parameter settings.

2 System Model

As depicted in Fig. 1, we investigate a CDRT system using backscatter NOMA, consisting of one BS, one RU, one CCU, and one CEU. In this system, it is feasible for the BS to communicate directly with RU and CCU. However, the BS can only communicate with the CEU with the assistance of RU. This is because the link between the BS and CEU has a long distance, severe deep fading, or obstruction. All nodes operate with a single antenna, and the RU employs a decode and forward (DF) protocol. Additionally, the BS is capable of full duplex communication, while the other nodes operate in half duplex mode. To improve the system spectral efficiency under the same energy supply conditions, each user node is equipped with a hybrid wireless circuit, which includes a transceiver circuit and a backscatter circuit. Specifically, the users can adaptively switch between transceiver mode and backscatter mode. In the transceiver mode, the users can complete general communication sending and receiving functions. When the users switch to backscatter mode, it can complete decoding of the received signals while reflecting its own information.

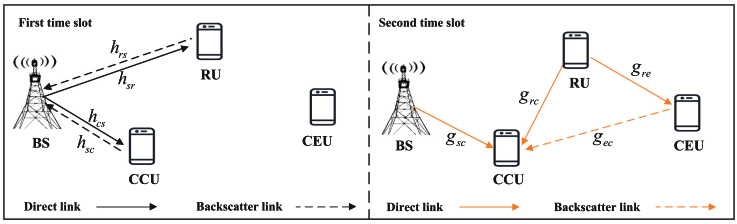

Fig. 1. Illustration of the considered system model.

Assume that all channel links experience quasi-static Rayleigh block fading. Subsequently, subscripts s, r, c, and e are used to denote the BS, RU, CCU, and CEU, while superscripts 1 and 2 are utilized to distinguish the first and second time slots, respectively. Define nodes w and v in the first time slot satisfy $w \in \{s, r, c\}$ and $v \in \{s, r, c\}$, nodes i and j in the second time slot meet $i \in \{s, r, e\}$ and $j \in \{c, e\}$. Let h_{wv} and H_{wv}, $w \neq v$, represent the channel coefficient and channel power between w and v in the first time slot, and let g_{ij} and G_{ij}, $i \neq j$, denote the channel coefficient and channel power between i and j in the second time slot. The channel coefficients h_{wv} and g_{ij} follow complex Gaussian distribution, i.e., $h_{wv} \sim CN(0, \Omega_{wv})$ and $g_{ij} \sim CN(0, \Omega_{ij})$. Without loss of generality, it is assumed that the channel configuration satisfies the conditions $\Omega_{sc} > \Omega_{sr}$, $\Omega_{cs} > \Omega_{rs}$, and $\Omega_{sc} > \Omega_{rc}$.

3 Transmission Protocol

3.1 First Time Slot

In the first time slot, the BS operates in full duplex mode and performs superposition coding on the power-normalized signals xc, xr, and x_e according to down-

link NOMA. The CCU and RU operate in the backscatter mode. The signals x_c, x_r, and x_e are needed by the CCU, RU, and CEU, respectively. The signal to be transmitted at the BS can be represented as $S_s^1 = \sqrt{\alpha_c}x_c + \sqrt{\alpha_r}x_r + \sqrt{\alpha_e}x_e$, where α_c, α_r, and α_e represent the power allocation coefficients (PACs) corresponding to the signals x_c, x_r, and x_e, respectively.

Due to $\Omega_{sc} > \Omega_{sr}$ and the absence of a direct link between the BS and the CEU, the PACs should meet $0 < \alpha_c < \alpha_r < \alpha_e < 1$ and $\alpha_e + \alpha_r + \alpha_c = 1$. The CCU and RU can leverage a fraction of the RF signals from the BS for backscatter modulation to convey their individual uplink signals u_c and u_r. Subsequently, the residual portion of the incoming signals can be used for self-information decoding. The received signals at the CCU, RU, and BS are given by $y_c^1 = h_{sc}\sqrt{(1-a_c)P_s}S_s^1 + n_c^1$, $y_r^1 = h_{sr}\sqrt{(1-a_r)P_s}S_s^1 + n_r^1$, and $y_s^1 = h_{sc}h_{cs}\sqrt{a_cP_s}S_s^1u_c + h_{sr}h_{rs}\sqrt{a_rP_s}S_s^1u_r + S_{\mathrm{SI}} + n_s^1$, respectively, where $0 < a_c < 1$ and $0 < a_r < 1$ are the reflection coefficients at the CCU and RU, and P_s is the transmit power at the BS. The term $n_w^1 \sim CN(0, \sigma^2)$ denotes the additive white Gaussian noise (AWGN) at the node $w \in \{s, c, r\}$. Moreover, $S_{\mathrm{SI}} \sim CN(0, \varepsilon P_s\Omega_{ss})$ is the self-interference term due to the full duplex, where $0 \le \varepsilon \le 1$ represents the residual interference level, and Ω_{ss} is the channel power of the self-interference channel of the BS.

According to downlink NOMA, the CCU needs to decode x_e, x_r, and x_c using successive interference cancellation (SIC). Thus, the signal-to-interference plus noise ratios (SINRs) for decoding x_e, x_r, and x_c at the CCU are given by

$$\gamma_{c,x_e}^1 = \frac{H_{sc}(1-a_c)\alpha_e\rho_s}{H_{sc}(1-a_c)(\alpha_c+\alpha_r)\rho_s + 1}, \tag{1}$$

$$\gamma_{c,x_r}^1 = \frac{H_{sc}(1-a_c)\alpha_r\rho_s}{H_{sc}(1-a_c)\alpha_c\rho_s + 1}, \tag{2}$$

$$\gamma_{c,x_c}^1 = H_{sc}(1-a_c)\alpha_c\rho_s, \tag{3}$$

where $\rho_s \triangleq \frac{P_s}{\sigma^2}$ represents the transmit SNR at the BS. Based on (3), the achievable rate associated with x_c is $R_{x_c} = \frac{1}{2}\log_2(1+\gamma_{c,x_c}^1)$. Meanwhile, the RU decodes the signals x_e and x_r via SIC, and the corresponding SINRs can be written as

$$\gamma_{r,x_e}^1 = \frac{H_{sr}(1-a_c)\alpha_e\rho_s}{H_{sr}(1-a_c)(\alpha_c+\alpha_r)\rho_s + 1}, \tag{4}$$

$$\gamma_{r,x_r}^1 = \frac{H_{sr}(1-a_c)\alpha_r\rho_s}{H_{sr}(1-a_c)\alpha_c\rho_s + 1}. \tag{5}$$

Since the CCU needs to successfully decode x_r in the first time slot before decoding x_c, the achievable rate for x_r is limited to γ_{c,x_r}^1. Based on (2) and (5), the achievable rate for x_r is given by $R_{x_r} = \frac{1}{2}\log_2(1 + \min\{\gamma_{c,x_r}^1, \gamma_{r,x_r}^1\})$.

By recalling y_s^1, the signal S_s^1 can be considered as a virtual fast fading channel gain for decoding u_c and u_r, where $S_s^1 \sim CN(0, 1)$. The process of the BS receiving the reflected uplink signals from the CCU and RU can be regarded as an uplink NOMA transmission. Due to $\Omega_{sc} > \Omega_{sr}$ and $\Omega_{cs} > \Omega_{rs}$, the reflection

coefficient is set to $a_c > a_r$. Thus, the BS can use SIC to decode u_c and u_r sequentially. The SINRs for the BS to decode u_c and u_r are given by

$$\gamma^1_{s,u_c} = \frac{H_{sc}H_{cs}a_c\rho_s|S^1_s|^2}{H_{sr}H_{rs}a_r\rho_s|S^1_s|^2 + \varepsilon\rho_s H_{ss} + 1}, \tag{6}$$

$$\gamma^1_{s,u_r} = \frac{H_{sr}H_{rs}a_r\rho_s|S^1_s|^2}{\varepsilon\rho_s H_{ss} + 1}, \tag{7}$$

where $H_{\mathrm{ss}} \sim \exp(\Omega_{ss})$. The achievable rates for u_c and u_r are given by $R_{u_c} = \frac{1}{2}\log_2(1+\gamma^1_{s,u_c})$ and $R_{u_r} = \frac{1}{2}\log_2(1+\gamma^1_{s,u_r})$, respectively.

3.2 Second Time Slot

In the second time slot, the CCU and RU switch to the transceiver mode, while the CEU operates in the backscatter mode. To fully utilize the time resources of the BS, a new downlink signal x'_c is transmitted to the CCU from the BS with the power P_s. The RU broadcasts the decoded signal x_e and the new signal x_{rc} by using superposition encoding with the transmit power P_r, where x_{rc} contains the environmental information that be collected for the CCU from the RU. Therefore, the superimposed encoded signal at the RU can be given by $S^2_r = \sqrt{\beta_{rc}}x_{rc} + \sqrt{\beta_e}x_e$, where β_{rc} and β_e denote the PACs corresponding to x_{rc} and x_e, respectively. Since the signal x_e is transmitted through a dual-hop link, the decoding requirement of x_e is higher than that of x_{rc}, the PACs should satisfy $0 < \beta_{rc} < \beta_e < 1$ and $\beta_{rc} + \beta_e = 1$. Assume that the normalized reflection coefficient at the CEU is b_e. The signal x_{ec} containing environmental information is loaded onto a part of received signal via backscatter modulation and reflected to the CCU. The remaining part of the received signal is used for information decoding. Based on this, the received signal at the CEU is given by $y^2_e = g_{re}\sqrt{(1-b_e)P_r}S^2_r + n^2_e$, where $P_r = \vartheta P_s$, $0 < \vartheta \leq 1$ denotes the power scaling factor, and $n^2_e \sim CN(0, N_0)$ is the AWGN at the CEU. The CEU decodes x_e by treating x_{rc} as interference, and the corresponding SINR is given by

$$\gamma^2_{e,x_e} = \frac{G_{re}(1-b_e)\beta_e\rho_r}{G_{re}(1-b_e)\beta_{rc}\rho_r + 1}, \tag{8}$$

where $\rho_r \triangleq \frac{P_r}{N_0}$ denotes the transmit SNR at the RU. In the first time slot, the CCU needs to decode x_e before performing SIC. Because the RU adopts the DF protocol, the achievable rate for x_e is constrained by the weaker link in the BS to RU and RU to CEU connections. Thus, by using (1), (4) and (8), the achievable rate for x_e is given by $R_{x_e} = \frac{1}{2}\log_2(1 + \min\{\gamma^1_{c,x_e}, \gamma^1_{r,x_e}, \gamma^2_{e,x_e}\})$.

The received signal at the CCU is written as $y^2_c = g_{sc}\sqrt{P_s}x'_c + g_{rc}\sqrt{P_r}S^2_r + g_{re}g_{ec}\sqrt{b_eP_r}S^2_r x_{ec} + n^2_c$, where $n^2_c \sim CN(0, \sigma^2)$ denotes the AWGN at the CCU. Since x_e has been decoded at the CCU in the first time slot, the CCU can utilize the side information of x_e to eliminate the term $g_{rc}\sqrt{\beta_eP_r}x_e$ in y^2_c. Furthermore, y^2_c is rewritten as $y^2_c = g_{sc}\sqrt{P_s}x'_c + g_{rc}\sqrt{\beta_{rc}P_r}x_{rc} + g_{re}g_{ec}\sqrt{b_eP_r}S^2_r x_{ec} + n^2_c$. The condition $\Omega_{sc} > \Omega_{rc}$ holds and P_s is usually higher than P_r. Besides, the

reflected signal x_{ec} experience a dual-fading channel, resulting in a corresponding lower received signal power level. Therefore, the decoding sequence of the SIC applied by the CCU is x'_c, x_{rc}, and x_{ec}. Specifically, the CCU first decodes x'_c by considering x_{rc} and x_{ec} as interference, with the corresponding SINR of

$$\gamma^2_{c,x'_c} = \frac{G_{sc}\rho_s}{G_{rc}\beta_{rc}\vartheta\rho_s + G_{re}G_{ec}b_e\vartheta\rho_s + 1}. \tag{9}$$

Similarly, the SINR for the CCU to decode x_{rc} can be given by

$$\gamma^2_{c,x_{rc}} = \frac{G_{rc}\beta_{rc}\vartheta\rho_s}{G_{re}G_{ec}b_e\vartheta\rho_s + 1}. \tag{10}$$

When decoding x_{ec}, the CCU treats S_r^2 as a known virtual fast fading channel coefficient. The corresponding SINR is given by

$$\gamma^2_{c,x_{ec}} = G_{re}G_{ec}b_e\vartheta\rho_s|S_r^2|^2. \tag{11}$$

Based on (9), (10) and (11), the achievable rates corresponding to the signal x'_c, x_{rc}, and x_{ec} are given by $R_{x'_c} = \frac{1}{2}\log_2(1+\gamma^2_{c,x'_c})$, $R_{x_{rc}} = \frac{1}{2}\log_2(1+\gamma^2_{c,x_{rc}})$, and $R_{x_{ec}} = \frac{1}{2}\log_2(1+\gamma^2_{c,x_{ec}})$, respectively.

4 Performance Analysis

This section analyzes the ESC for the proposed scheme. Because this paper considers Rayleigh block fading channels and assumes that $S_s^1 \sim CN(0,1)$ and $S_r^2 \sim CN(0,1)$ hold, both the channel power and signal power follow exponential distributions. Using (3) and R_{x_c}, the ergodic capacity for x_c is calculated as

$$\begin{aligned} C_{x_c} &= \frac{1}{2\ln 2}\int_0^\infty \frac{1}{1+x}\big(1 - F_{\gamma^1_{c,x_c}}(x)\big)dx \\ &= \frac{1}{2\ln 2}\int_0^\infty \frac{1}{1+x} e^{-\frac{v}{(1-a_c)\alpha_c\rho_s\Omega_{sc}}}dx \\ &= -\frac{1}{2\ln 2} e^{\frac{1}{(1-a_c)\alpha_c\rho_s\Omega_{sc}}}\mathrm{Ei}(-1/((1-a_c)\alpha_c\rho_s\Omega_{sc})), \end{aligned} \tag{12}$$

where $\mathrm{Ei}(\cdot)$ is the exponential integral function [[11], eq.3.352.4].

Let $Z_1 \triangleq \min\{\gamma^1_{c,x_r}, \gamma^1_{r,x_r}\}$. Based on the order statistics, the cumulative distribution function (CDF) of Z_1 is obtained as $F_{Z_1}(z) = 1 - (1 - F_{\gamma^1_{c,x_r}}(z))(1 - F_{\gamma^1_{c,x_r}}(z))$, where $F_{\gamma^1_{c,x_r}}(x) = 1 - \exp\big(-\frac{x}{(1-a_c)\rho_s\Omega_{sc}(\alpha_r - \alpha_c x)}\big)$ and $F_{\gamma^1_{r,x_r}}(x) = 1 - \exp\big(-\frac{x}{(1-a_c)\rho_s\Omega_{sr}(\alpha_r - \alpha_c x)}\big)$ for $x < \frac{\alpha_r}{\alpha_c}$, while $F_{\gamma^1_{c,x_r}}(x) = 1$ and $F_{\gamma^1_{r,x_r}}(x) = 1$ for $x \geq \frac{\alpha_r}{\alpha_c}$. Therefore, using Gaussian-Chebyshev quadrature, the ergodic capacity for x_r is given by

$$\begin{aligned} C_{x_r} &= \frac{1}{2\ln 2}\int_0^{\frac{\alpha_r}{\alpha_c}} \frac{1}{1+z}(1 - F_{Z_1}(z))dz \\ &= \frac{\alpha_r\pi}{4\ln 2\alpha_c M_{x_r}} \sum\nolimits_{m_{x_r}=1}^{M_{x_r}} \sqrt{1 - {Q_{x_r}}^2}(1 - F_{Z_1}(q_{x_r}))\frac{1}{1+q_{x_r}}, \end{aligned} \tag{13}$$

where $Q_{x_r} = \cos(\frac{2m_{x_r}-1}{2M_{x_r}}\pi)$, $q_{x_r} = \frac{\alpha_r(1+Q_{x_r})}{2\alpha_c}$, M_{x_r} is a complexity-accuracy tradeoff parameter.

Let $Z_2 \triangleq \min\{\gamma^1_{c,x_e}, \gamma^1_{r,x_e}, \gamma^2_{e,x_e}\}$. Similar to Z_1, applying the order statistics, then we can calculate the CDF of Z_2 as $F_{Z_2}(z) = 1-(1-F_{\gamma^1_{c,x_e}}(z))(1-F_{\gamma^1_{r,x_e}}(z))(1-F_{\gamma^2_{e,x_e}}(z))$, where $F_{\gamma^1_{c,x_e}}(x) = 1-\exp\left(-\frac{x}{(\alpha_e-(\alpha_c+\alpha_r)x)(1-a_c)\rho_s\Omega_{sc}}\right)$ and $F_{\gamma^1_{r,x_e}}(x) = 1-\exp\left(-\frac{x}{(\alpha_e-(\alpha_c+\alpha_r)x)(1-a_c)\rho_s\Omega_{sr}}\right)$ for $x < \frac{\alpha_e}{\alpha_c+\alpha_r}$, while $F_{\gamma^1_{c,x_e}}$ and $F_{\gamma^1_{r,x_e}}(x)$ equal one for $x \geq \frac{\alpha_e}{\alpha_c+\alpha_r}$. The CDF of γ^2_{e,x_e} is $F_{\gamma^2_{e,x_e}}(x) = 1-\exp\left(-\frac{x}{(1-b_e)\rho_r(\beta_e-\beta_{rc}x)\Omega_{re}}\right)$ and $F_{\gamma^2_{e,x_e}}(x) = 1$ for $x < \frac{\beta_e}{\beta_{rc}}$ and $x \geq \frac{\beta_e}{\beta_{rc}}$, respectively. Therefore, using Gaussian-Chebyshev quadrature, the ergodic capacity for x_e can be obtained as

$$\begin{aligned} C_{x_e} &= \frac{1}{2\ln 2}\int_0^{\varphi_{x_e}} \frac{1}{1+z}(1-F_{Z_2}(z))dz \\ &= \frac{\varphi_{x_e}\pi}{4\ln 2 M_{x_e}} \sum\nolimits_{m_{x_e}=1}^{M_{x_e}} \sqrt{1-{Q_{x_e}}^2}(1-F_{Z_2}(q_{x_e}))\frac{1}{1+q_{x_e}}, \end{aligned} \tag{14}$$

where $\varphi_{x_e} = \min\{\frac{\alpha_e}{\alpha_c+\alpha_r}, \frac{\beta_e}{\beta_{rc}}\}$, $Q_{x_e} = \cos(\frac{2m_{x_e}-1}{2M_{x_e}}\pi)$, $q_{x_e} = \frac{\varphi_{x_e}(1+Q_{x_e})}{2}$, and M_{x_e} denotes the complexity-accuracy tradeoff parameter.

Theorem 1. *The ergodic capacity for u_c can be written as*

$$C_{u_c} = \Xi_{11} - \Xi_{12} - \Xi_2, \tag{15}$$

where

$$\begin{aligned} \Xi_{11} =& -\frac{1}{2\ln 2}\frac{\pi^2}{4M_{\Xi_{11}}} \sum\nolimits_{m_{\Xi_{11}}=1}^{M_{\Xi_{11}}} \sqrt{1-{Q_{\Xi_{11}}}^2} e^{\frac{1}{2\tan q_{\Xi_{11}}}} \\ &\times \mathrm{Ei}(-1/(2\tan q_{\Xi_{11}}))f_{V_1}(\tan q_{\Xi_{11}})(\sec q_{\Xi_{11}})^2, \end{aligned} \tag{16}$$

$$\begin{aligned} \Xi_{12} =& \frac{\pi^4}{64\ln 2 M_{\theta'}M_\theta} \sum\nolimits_{m_{\theta'}=1}^{M_{\theta'}} \sum\nolimits_{m_\theta=1}^{M_\theta} \sqrt{1-(Q_{\theta'})^2}\sqrt{1-(Q_\theta)^2} \\ &\times e^{\frac{1+\tan q_{\theta'}}{\varepsilon\rho_s\Omega_{ss}} - \frac{\tan q_{\theta'}}{2\tan q_\theta}} \mathrm{Ei}\Big(-\frac{1+\tan q_{\theta'}}{\varepsilon\rho_s\Omega_{ss}}\Big)\frac{1}{\tan q_\theta}(\sec q_{\theta'})^2(\sec q_\theta)^2 f_{V_1}(\tan q_\theta), \end{aligned} \tag{17}$$

$$\Xi_2 = \Xi_1(f_{V_1}(\cdot) \to f_{V_2}(\cdot)), \tag{18}$$

where $f_{V_1}(v) = 2\sum_{j_1=1}^{2}\left\{\prod_{\substack{j_2=1\\ j_2\neq j_1}}^{2} \frac{\tilde{\Omega}'_{j_1}}{\tilde{\Omega}'_{j_1}-\tilde{\Omega}'_{j_2}}(\frac{2}{\tilde{\Omega}'_{j_1}})^{\frac{3}{2}} v^{\frac{1}{2}} K_1(2\sqrt{\frac{2}{\tilde{\Omega}'_{j_1}}v})\right\}$, $f_{V_2}(v) = \frac{2}{\tilde{\Omega}_{sr}}K_0(2\sqrt{\frac{v}{\tilde{\Omega}_{sr}}})$, *and* $(f_{V_1}(\cdot) \to f_{V_2}(\cdot))$ *represent that* Ξ_2 *can be obtained by replacing* $f_{V_1}(\cdot)$ *to* $f_{V_2}(\cdot)$ *in* Ξ_1. *The functions* $K_1(\cdot)$ *and* $K_0(\cdot)$ *represent the first-order and zero-order modified Bessel functions of the second kind, respectively. Besides,* $Q_\theta = \cos(\frac{2m_\theta-1}{2M_\theta}\pi)$, $Q_{\theta'} = \cos(\frac{2m_{\theta'}-1}{2M_{\theta'}}\pi)$, $Q_{\Xi_{11}} = \cos(\frac{2m_{\Xi_{11}}-1}{2M_{\Xi_{11}}}\pi)$, $q_{\Xi_{11}} = \frac{\pi(1+Q_{\Xi_{11}})}{4}$, $q_\theta = \frac{\pi}{4}(1+Q_\theta)$, *and* $q_{\theta'} = \frac{\pi}{4}(1+Q_{\theta'})$, *where* $M_{\theta'}$, M_θ, *and* $M_{\Xi_{11}}$ *are complexity-tradeoff parameters.*

Proof. See Appendix A. □

Using a derivation method similar to Theorem 1, we can calculate C_{u_r} as $C_{u_r} = \Xi_2 - \Xi_3$, where $\Xi_3 = -\frac{1}{2\ln 2} e^{\frac{1}{\varepsilon\rho_s\Omega_{ss}}} \mathrm{Ei}(-\frac{1}{\varepsilon\rho_s\Omega_{ss}})$. Applying the Gaussian-Chebyshev quadrature with variable substitution $x = \tan\theta$,we can approximate the ergodic capacity for x'_c as

$$\begin{aligned} C_{x'_c} &= \frac{1}{2\ln 2}\int_0^{\frac{\pi}{2}} \frac{1 - F_L(\tan\theta)}{1+\tan\theta}(\sec\theta)^2 d\theta \\ &= \frac{1}{2\ln 2}\frac{\pi^2}{4M_{x'_c}} \sum\nolimits_{m_{x'_c}=1}^{M_{x'_c}} \sqrt{1-Q_{x'_c}{}^2}\frac{1-F_L(\tan q_{x'_c})}{1+\tan q_{x'_c}}(\sec q_{x'_c})^2, \end{aligned} \tag{19}$$

where $F_L(l) = 1 + \frac{\Omega_{sc}{}^2}{(\Omega_{rc}\beta_{rc}\vartheta l + \Omega_{sc})\Omega_{re}\Omega_{ec}b_e\vartheta l} e^{\frac{\Omega_{sc}}{\Omega_{re}\Omega_{ec}b_e\vartheta l} - \frac{l}{\Omega_{sc}\rho_s}} \mathrm{Ei}(-\frac{\Omega_{sc}}{\Omega_{re}\Omega_{ec}b_e\vartheta l})$, $Q_{x'_c} = \cos(\frac{2m_{x'_c}-1}{2M_{x'_c}}\pi)$, $q_{x'_c} = \frac{\pi}{4}(1+Q_{x'_c})$, and $M_{x_{c'}}$ is a accuracy-complexity tradeoff parameter.

Similarly, using [[11], 3.352.4], the variable substitution $x = \tan\theta$, and Gaussian-Chebyshev quadrature, we can calculate $C_{x_{ec}}$ as

$$\begin{aligned} C_{x_{ec}} =& \frac{1}{2\ln 2}\int_0^{\infty}\int_0^{\infty} e^{-\frac{u}{b_e\vartheta\rho_s x}}/(1+u) f_{G_{re}G_{ec}}(x)du \\ =& \frac{1}{2\ln 2}\int_0^{\infty} -e^{\frac{1}{b_e\vartheta\rho_s x}}\mathrm{Ei}(-\frac{1}{b_e\vartheta\rho_s x}) f_{G_{re}G_{ec}}(x)dx \\ =& -\frac{1}{2\ln 2}\frac{\pi^2}{4M_{x_{ec}}}\sum\nolimits_{m_{x_{ec}}=1}^{M_{x_{ec}}}\sqrt{1-Q_{x_{ec}}{}^2}e^{\frac{1}{b_e\vartheta\rho_s\tan q_{x_{ec}}}} \\ &\times \mathrm{Ei}(-\frac{1}{b_e\vartheta\rho_s\tan q_{x_{ec}}}) f_{G_{re}G_{ec}}(\tan q_{x_{ec}})(\sec(q_{x_{ec}}))^2, \end{aligned} \tag{20}$$

where $Q_{x_{ec}} = \cos(\frac{2m_{x_{ec}}-1}{2M_{x_{ec}}}\pi)$, $q_{x_{ec}} = \frac{\pi}{4}(1+Q_{x_{ec}})$, $f_{|S_r^2|^2}(x) = e^{-x}$, $f_{G_{re}G_{ec}}(x) = \frac{2}{\Omega_{re}\Omega_{ec}} K_0\left(2\sqrt{\frac{x}{\Omega_{re}\Omega_{ec}}}\right)$, and $M_{x_{ec}}$ is a accuracy-complexity tradeoff parameter.

Similarly, the ergodic rate for x_{rc} can be calculated as

$$\begin{aligned} C_{x_{rc}} =& \frac{1}{2\ln 2}\int_0^{\infty}\frac{1-F_T(t)}{1+t}dt \\ =& \frac{\pi^2}{8\ln 2 M_{x_{rc}}}\sum\nolimits_{m_{x_{rc}}=1}^{M_{x_{rc}}}\sqrt{1-Q_{x_{rc}}{}^2}\frac{1-F_T(\tan q_{x_{rc}})}{1+\tan q_{x_{rc}}}(\sec q_{x_{rc}})^2, \end{aligned} \tag{21}$$

where $F_T(t) = 1 + \frac{\beta_{rc}\Omega_{rc}}{b_e\Omega_{re}\Omega_{ec}t} e^{\frac{\beta_{rc}\Omega_{rc}}{b_e\Omega_{re}\Omega_{ec}t} - \frac{t}{\beta_{rc}\vartheta\rho_s\Omega_{rc}}} \mathrm{Ei}(-\frac{\beta_{rc}\Omega_{rc}}{b_e\Omega_{re}\Omega_{ec}t})$, $q_{x_{rc}} = \frac{\pi}{4}(1 + Q_{x_{rc}})$, $Q_{x_{rc}} = \cos(\frac{2m_{x_{rc}}-1}{2M_{x_{rc}}}\pi)$, and $M_{x_{rc}}$ is a accuracy-complexity tradeoff parameter. Based on the above analysis, the ESC for the proposed scheme is given by $C_{\mathrm{sum}} = C_{x_c} + C_{x_r} + C_{x_e} + C_{u_c} + C_{u_r} + C_{x'_c} + C_{x_{ec}} + C_{x_{rc}}$.

5 Simulation Results

This section evaluates the ESC of the proposed scheme (i.e., Prop.), the conventional NOMA based CDRT (i.e., CNC), and OMA under the same parameter

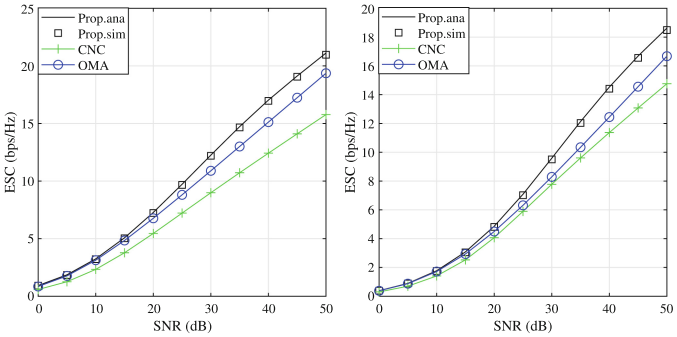

Fig. 2. ESC versus transmit SNR in two cases

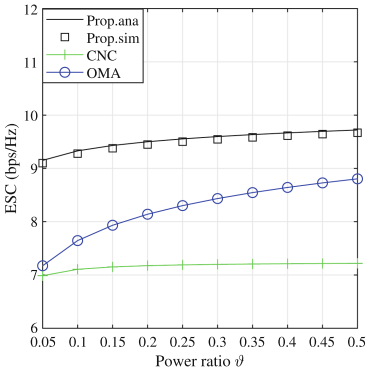

Fig. 3. ESC versus power ratio ϑ in Case I.

settings. We consider two cases, where Case I is set to $\Omega_{sc} = \Omega_{cs} = \Omega_{ss} = 1$, $\Omega_{sr} = \Omega_{rs} = \Omega_{rc} = \Omega_{re} = \Omega_{ec} = 0.8$, and $\vartheta = 0.5$, and Case II is set to $\Omega_{sc} = \Omega_{cs} = \Omega_{re} = \Omega_{ec} = 0.5$, $\Omega_{sr} = \Omega_{rs} = \Omega_{rc} = 0.25$, $\Omega_{ss} = 1$, and $\vartheta = 0.1$. The PACs are set to $\alpha_c = 0.01$, $\alpha_r = 0.09$, $\alpha_e = 0.9$, $\beta_e = 0.9$, and $\beta_{rc} = 0.1$. The reflection coefficients are set to $a_c = a_r = a_e = 0.6$. For fair comparison, the PACs for the NOMA-based CDRT are consistent with the proposed scheme.

Figure 2 illustrates the relationship between the ESC and ρ_s. The figure shows a significant overlap between the simulated values and the theoretical curves, which indicates the correctness of the theoretical analysis. Moreover, the proposed scheme outperforms other benchmarks in terms of ESC in different cases. This is because the proposed scheme simultaneously applies NOMA and backscatter communication to the system, which improves the system ESC. Since OMA transmits as many signals as the proposed scheme without inter-user interference, it can achieve higher ESC than the CNC. Figure 3 depicts the ESC under different power ratio ϑ. From the figure, it can be seen that the proposed scheme still achieves the best ESC with ϑ. As the ρ_r increases, the ESCs

for all the three schemes are improved to different degrees. This is due to the fact that the increase of transmit power at the RU can improve the information rate of the CEU in all the schemes, thus increasing the overall ESC.

6 Conclusions

This paper investigated a NOMA based CDRT system comprising one full duplex BS, one RU, one CCU, and one CEU. To enhance the system SE, we proposed a bidirectional backscatter NOMA scheme, wherein the BS employs downlink NOMA and uplink NOMA to serve three users and collect information from the RU and CCU. Simultaneously, the CCU collects information from the RU and CEU. The closed-form expressions for the ESC of the proposed scheme were derived to evaluate system performance. Simulation results demonstrate that the proposed analytical framework accurately characterizes system performance. Moreover, the ESC performance of the proposed scheme outperforms both the NOMA-based CDRT and OMA schemes.

A Proof of Theorem 1

Denote $A \triangleq H_{sr}H_{rs}a_r\rho_s|S_s^1|^2+H_{sc}H_{cs}a_c\rho_s|S_s^1|^2=|\sum_{n=1}^{2}\tilde{h}_n\hat{h}_n\sqrt{a_n\rho_s}S_s^1|^2$, $B \triangleq H_{sr}H_{rs}a_r\rho_s|S_s^1|^2$, and $C \triangleq \varepsilon\rho_s H_{ss}$, where $\tilde{h}_1 = h_{sr}$, $\hat{h}_1 = h_{rs}$, $\tilde{h}_2 = h_{sc}$, $\hat{h}_2 = h_{cs}$, $a_1 = a_r$, and $a_2 = a_c$. Based on this, the probability density functions (PDFs) of A, B, and C can be written as $f_A(a) = \frac{1}{2V_1}e^{-\frac{a}{2V_1}}$, $f_B(b) = \frac{1}{2V_2}e^{-\frac{b}{2V_2}}$, and $f_C(c) = \frac{1}{\varepsilon\rho_s\Omega_{ss}}e^{-\frac{c}{\varepsilon\rho_s\Omega_{ss}}}$, where $V_1 = \frac{\sum_{n=1}^{2}a_n\rho_s|\tilde{h}_n\hat{h}_n|^2}{2}$ and $V_2 = \frac{a_r\rho_s|h_{sr}h_{rs}|^2}{2}$. Based on γ_{s,u_c}^1, the ESC for u_c can be rewritten as

$$\begin{aligned} C_{u_c} =& \frac{1}{2\ln 2}E\left\{\ln(A+C+1)-\ln(B+C+1)\right\} \\ =& \underbrace{\frac{1}{2\ln 2}\int_0^\infty\int_0^\infty\int_0^\infty \ln(a+c+1)f_A(a)f_C(c)f_{V_1}(v)dadcdv}_{\Xi_1} \\ &- \underbrace{\frac{1}{2\ln 2}\int_0^\infty\int_0^\infty\int_0^\infty \ln(b+c+1)f_B(b)f_C(c)f_{V_2}(v)dbdcdv}_{\Xi_2}. \end{aligned} \tag{22}$$

Considering A as a function of variable S_s^1, we have $\mathrm{Re}\{\sum_{n=1}^{2}\tilde{h}_n\hat{h}_n\sqrt{a_n\rho_s}S_s^1\} \sim N(0,V_1)$ and $\mathrm{Im}\{\sum_{n=1}^{2}\tilde{h}_n\hat{h}_n\sqrt{a_n\rho_s}S_s^1\} \sim N(0,V_1)$. Specifically, V_1 and V_2 can be equivalently written as $V_1 = \sum_{n=1}^{2}|\tilde{h}_n'\hat{h}_n'|^2$ and $V_2 = |\tilde{h}_{sr}\hat{h}_{rs}|^2$, where $\tilde{h}_n' \sim CN(0,\tilde{\Omega}_n')$, $\hat{h}_n' \sim CN(0,1)$, $\tilde{h}_{sr} \sim CN(0,\tilde{\Omega}_{sr})$, $\hat{h}_{rs} \sim CN(0,1)$, $\tilde{\Omega}_n' = \frac{a_n\rho_s\tilde{\Omega}_n\hat{\Omega}_n}{2}$, and $\tilde{\Omega}_{sr} = \frac{a_r\rho_s\Omega_{sr}\Omega_{rs}}{2}$. According to [12], the PDFs of V_1 and V_2 are given in

Theorem 1. Substituting $f_C(c)$ and [[11], 4.337.1] to (22), we have

$$\Xi_1 = \underbrace{\frac{1}{2\ln 2}\int_0^\infty \int_0^\infty \ln(1+a) f_A(a) f_{V_1}(v) da dv}_{\Xi_{11}} - \underbrace{\frac{1}{2\ln 2}\int_0^\infty \int_0^\infty e^{\frac{1+a}{\varepsilon \rho_s \Omega_{ss}}} \mathrm{Ei}\left(-\frac{1+a}{\varepsilon \rho_s \Omega_{ss}}\right) f_A(a) f_{V_1}(v) da dv}_{\Xi_{12}}. \quad (23)$$

Furthermore, applying [[11], 4.337.1], the variable substitution $\theta = \arctan v$, and the Gaussian-Chebyshev quadrature to Ξ_{11}, we can obtain Ξ_{11} as (16). Similarly, we can use the variable substitutions $\theta = \arctan v$ and $\theta' = \arctan a$, and the Gaussian-Chebyshev quadrature to obtain Ξ_{12} as (17). Since Ξ_1 and Ξ_2 have similar integral forms, we can easily obtain $\Xi_2 = \Xi_1(f_{V_1}(\cdot) \to f_{V_2}(\cdot))$. Substituting Ξ_{11}, Ξ_{12}, and Ξ_2 into (19), we obtain C_{u_c}.

References

1. Han, S., Li, Z., Xue, Q., Meng, W., Li, C.: Joint broadcast and unicast transmission based on RSMA and spectrum sharing for integrated satellite-terrestrial network. IEEE Trans. Cognitive Commun. Netw. (2024). https://doi.org/10.1109/TCCN.2024.3350596
2. Zhang, R., et al.: Integrated sensing and communication with massive MIMO: a unified tensor approach for channel and target parameter estimation. IEEE Trans. Wireless Commun. (2024). https://doi.org/10.1109/TWC.2024.3351856 Early Access
3. Wu, C., You, C., Liu, Y., Han, S., Renzo, M.D.: Two-timescale design for STAR-RIS-aided NOMA systems. IEEE Trans. Commun. **72**(1), 585–600 (2024)
4. Kim, J.-B., Lee, I.-H.: Non-orthogonal multiple access in coordinated direct and relay transmission. IEEE Wireless Commun. Lett. **19**(11), 2037–2040 (2015)
5. Xu, Y., et al.: Coordinated direct and relay transmission with NOMA and network coding in Nakagami-m fading channels. IEEE Trans. Commun. **69**(1), 207–222 (2021)
6. Xu, Y., Cheng, J., Wang, G., Leung, V.C.M.: Adaptive coordinated direct and relay transmission for NOMA networks: a joint downlink-uplink scheme. IEEE Trans. Wireless Commun. **20**(7), 4328–4346 (2021)
7. Lei, H., et al.: On secure CDRT with NOMA and physical-layer network coding. IEEE Trans. Commun. **71**(1), 381–396 (2023)
8. Xu, Y., Du, Z., Yuan, W., Jia, S., Leung, V.C.M.: Performance of OTFS-NOMA scheme for coordinated direct and relay transmission networks in high-mobility scenarios. IEEE Wireless Commun. Lett. **12**(12), 2268–2272 (2023)
9. Liang, Y.-C., Long, R., Zhang, Q., Niyato, D.: Symbiotic communications: where Marconi meets Darwin. IEEE Wireless Commun. **29**(1), 144–150 (2022)
10. Chen, W., et al.: Backscatter cooperation in NOMA communications systems. IEEE Trans. Wireless Commun. **20**(6), 3458–3474 (2021)

11. Gradshteyn, I.S., Ryzhik, I.M.: Tables of Integrals, Series, and Products, 7th edn. Academic Press, New York (2007)
12. Chatzidiamantis, N.D., Karagiannidis, G.K.: On the distribution of the sum of gamma-gamma variates and applications in RF and optical wireless communications. IEEE Trans. Commun. **59**(5), 1298–1308 (2011)